Nanostructures

A General Route to Macroscopic Hierarchical 3D Nanowire Networks**

Donghai Wang, Hongmei Luo, Rong Kou, Maria P. Gil, Shuaigang Xiao, Vladimir O. Golub, Zhenzhong Yang, C. Jeffrey Brinker, and Yunfeng Lu**

Nanoscale building blocks, such as equiaxial nanocrystals, one-dimensional nanotubes, wires, and rods, and 3D nano-

[*] D. Wang, H. Luo, R. Kou, M. P. Gil, Prof. Y. Lu
Department of Chemical and Biomolecular Engineering
Tulane University
New Orleans, LA 70118 (USA)
Fax: (+1) 504-865-6744
E-mail: ylu@tulane.edu

S. Xiao
Department of Chemical and Biological Engineering
University of Wisconsin
Madison, Wisconsin 53706 (USA)

Dr. V. O. Golub
Advanced Materials Research Institute
University of New Orleans
New Orleans, LA 70118 (USA)

Prof. Z. Yang
State Key Laboratory of Polymer Physics and
Chemistry Joint Laboratory of Polymer Science and Materials
Institute of Chemistry
Chinese Academy of Science
Beijing, 100080 (P. R. China)
Fax: (+86) 10-6255-9373
E-mail: yangzz@iccas.ac.cn

Prof. C. J. Brinker
Sandia National Laboratories and
The University of New Mexico
1001 University Blvd. SE
Albuquerque, NM 87106 (USA)

[**] The work was partially funded by NASA (Grants NAG-1-02070 and NCC-3-946), the Office of Naval Research, Louisiana Board of Regents (Grant LEQSF(2001-04)-RD-B-09), the National Science Foundation (Grant NSF-DMR-0124765 and CAREER Award), and the National Science Foundation of China (Grants 50325313 and 20128004). We thank Dr. Jibao He for help with TEM imaging measurements.

Supporting information for this article is available on the WWW under http://www.angewandte.org or from the author.

 DOI: 10.1002/anie.200460535

structures, such as nanomesh and superlattices, have been studied intensively not only because of their interesting intrinsic properties, which arise from low dimensionality and quantum effects, but also their capability for direct nanosystem integration. To date, nanoscale building-block assemblies for applications such as nanocomputing and nanophotonics have been developed by using microfluidic,[1] Langmuir–Blodgett,[2] and other techniques.[3] These 2D structures that are assembled through weak noncovalent interactions[4,5] or external fields (e.g. shearing[6] and electric fields[3]) are unsuitable for devices that require intensive interwire communications (e.g. efficient charge transport), high surface areas, excellent accessibility, and mechanical robustness. Fabrication of 3D nanowire networks with controlled diameters and arrangements of the wire, tailored pore structures, and effective interwire connectivity is therefore paramount for new device applications. Current inverse opal networks[7] are limited by the large diameters of the wire that may preclude quantum effects, and recent biomimetic approaches have also resulted in networks of large, randomly connected wires.[8]

We report here a general synthetic route to stable, 3D continuous, hierarchically organized networks of metals or semiconductors that are composed of nanowire-like elements which uses a templated electrodeposition technique. Although reverse surfactant liquid-crystalline[9] and 2D hexagonal mesoporous silica templates[10] have been used to electrochemically deposit 2D nanowires, removal of the templates has resulted in aggregated nanowires with poor structural control. Here we have electrochemically replicated the bicontinuous surfactant liquid-crystalline (LC) phases to obtain a robust nanowire network. Figure 1 outlines the approach: first, a film of mesoporous silica is coated onto a conductive substrate through the co-assembly of the silicate and surfactant molecules followed by removal of the surfactant,[11] then, the pore channels are filled with metals or semiconductors by electrodeposition, and lastly, the silica template is removed to create a replicated mesoporous nanowire network. Besides the excellent control over the composition, this approach enables precise structural tuning by replication of the complicated but well-studied silicate/surfactant LC mesophases. For example, the diameter of the nanowire can be tuned from 2 to 20 nm depending on the pore sizes of the template, and 3D networks of nanowires can be controlled by the 3D cubic mesostructure. Pore sizes of the nanowire networks can be tuned from 1 to 4 nm depending on the thickness of the pore walls of the templates.[12,13] Hierarchical pore structures can be readily obtained by the incorporation of colloidal silica porogens, which range in size from a few to several hundred nanometers, or by the incorporation of templates with various shapes, such as particles, rods, and plates, into the self-assembled surfactant/silicate mesophases followed by their removal.

The replication of ordered 3D crystalline nanowire networks can be analyzed by transmission electron microscopy (TEM) and X-ray diffraction (XRD) measurements. Figure 2, a–c show TEM images of cubic mesoporous templates, which were prepared by using Brij 58 surfactant (unit cell parameter of 8.4 nm), along the [111], [211], and [100] orientations. The diameter and wall thickness of the pores of the templates were estimated from nitrogen sorption, XRD, and TEM studies to have values of around 4–6 nm and 2–3 nm, respectively. Small angle XRD shows the presence of a (211) reflection, which corresponds to a d-spacing of 34.6 Å, for both the nanowire networks and the template and indicates good fidelity of the replication process. The broadening of the (211) reflection and the absence of the (210) reflection from the nanowire networks are due to a partial destruction of long-range mesostructural order upon removal of the template (see Supporting Information). Figure 2, d–f show TEM images of the replicated Pd (parts d and e) and Pt (part f) 3D nanowire networks. The average diameters of the nanowire (5 nm) and the pore (2–3 nm) agree well with the pore sizes (4–6 nm) and pore-wall thickness (2–3 nm), respectively, of the templates. The crystalline lattice of the Pt nanowire networks is clearly revealed in the high-resolution TEM (HRTEM) image (Figure 2 g). The ring patterns from selected area electron diffraction (SAED) studies of the Pd and Pt nanowire networks (insets of Figure 2 d and f, respectively) indicate that these nanowire networks possess randomly oriented *fcc* crystalline domains. The crystallite sizes estimated from XRD and TEM are ≈ 5 nm, which is similar to the pore size of the template.

Macroscopic connectedness of the networks was confirmed by field emission scanning electron microscopy (FESEM) studies as shown in Figure 3. The Pt nanowire network shows a continuous, homogeneous surface morphology (Figure 3 a) with an ordered mesostructure (Figure 3 b). Electronic continuity was demonstrated by cyclic voltammetry measurements performed upon an acidic aqueous solution in which hydrogen adsorption–desorption occurred at the surface of the Pt nanowire (Figure 4 a). The charge associated with hydrogen adsorption and oxidation is proportional to the active surface area of the Pt nanowire network. By this approach, an average active surface area of $27 \pm 2\ m^2 g^{-1}$ was determined, which is comparable to that of mesoporous Pt.[14] Three anodic hydrogen oxidation peaks were present at relative potentials of 0.03, −0.03, and −0.08 V (vs.

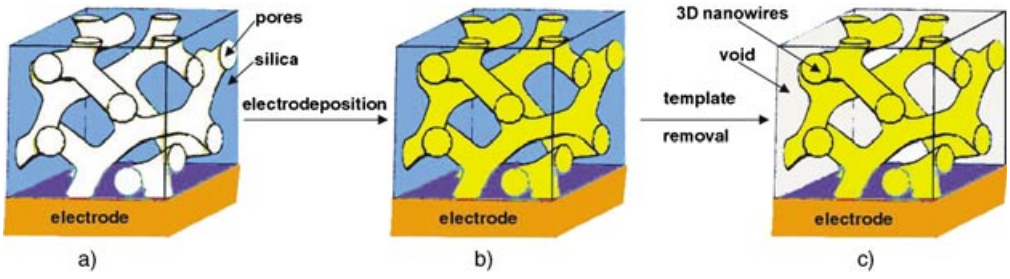

Figure 1. Schematic showing the formation of 3D continuous macroscopic metal or semiconductor nanowire networks by a templated electrodeposition technique. a) 3D cubic mesoporous template, b) 3D nanowire/silica nanocomposites, c) 3D nanowire network.

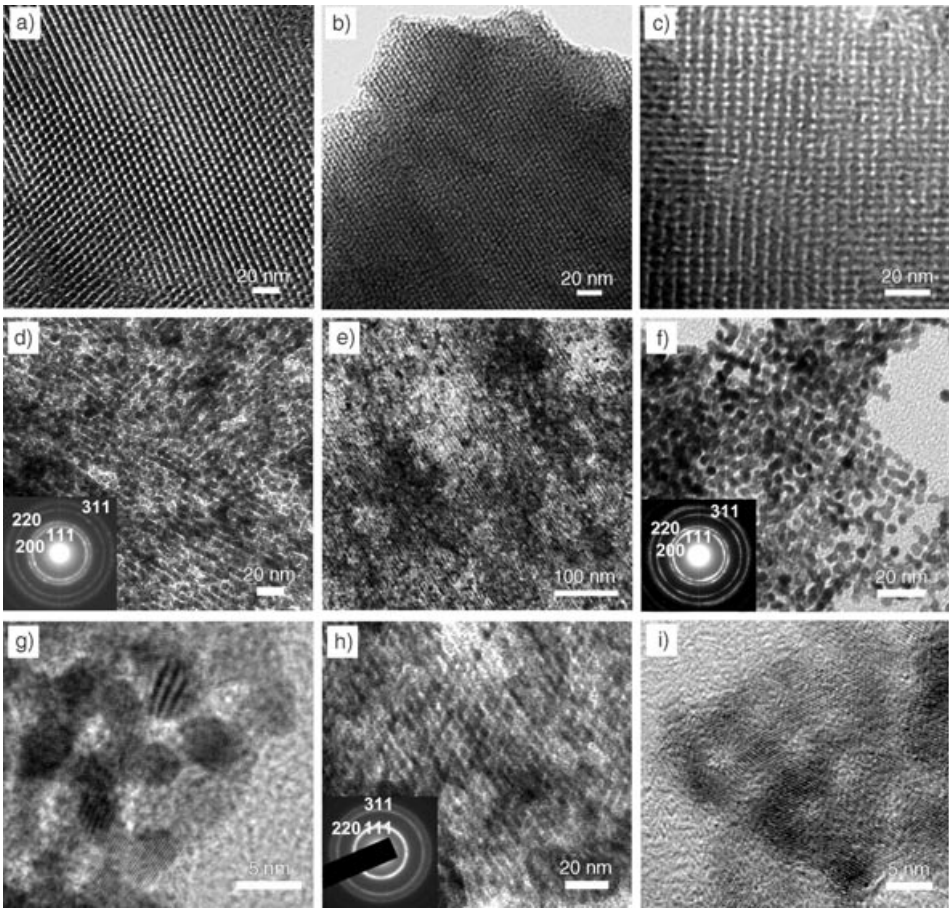

Figure 2. TEM images of the 3D cubic mesoporous silica templates prepared using Brij 58 surfactant, and the replicated metal or semiconductor nanowire networks. a), b), and c) TEM images of the cubic structured template along the [111], [211], and [100] directions, respectively. The pore-to-pore distances measured from the TEM images are ≈4.8, 3.4, and 8.2 nm, respectively, and agree well with the results of XRD studies ($a = 8.4$ nm). d) and e) TEM images of the Pd nanowire network replicas along the [111] and [211] directions, respectively, which indicate the formation of a highly ordered Pd nanowire network; the inset in (d) shows a SAED pattern of the Pd nanowire network with a typical Pd *fcc* crystal structure. f) TEM image of a Pt nanowire network replica along the [100] direction; the inset in (f) shows the SAED pattern of the Pt nanowire network with a typical Pt *fcc* crystal structure. g) HRTEM image of a Pt nanowire network. h) TEM image of a [111]-oriented CdSe nanowire network; the inset of (h) shows the SAED pattern of a polycrystalline CdSe network with a randomly oriented crystalline structure. i) HRTEM image of a CdSe nanowire network showing crystalline lattice fringes.

SCE, saturated calomel electrode), which is consistent with the isotropic polycrystalline nature of the nanowire network. The cyclic voltammetry studies demonstrate catalytic activity, pore accessibility, and electrical continuity of the nanowire networks.

Device applications often require hierarchical pore structures that may provide higher surface areas and more-efficient mass transport. The strategy presented here has particular advantages in the preparation of such hierarchical nanowire networks because silica templates with hierarchical structures can easily be made through the surfactant–assembly process.[15] For example, hierarchical templates used in this research were prepared by the introduction of colloidal silica spheres (20–100-nm diameters) into the surfactant/silicate thin-film assemblies, followed by calcination. Electrodeposition and template removal resulted in the hierarchical nanowire networks shown in Figure 3, c–e. FESEM and TEM images (Figure 3, d and e, respectively) of the hierarchical Pt nanowire networks clearly indicate the formation of secondary pores (20–100 nm). Highly porous nanowire networks with spongelike (Figure 3c) and grasslike (Figure 3e) morphologies are clearly revealed. As the silica particles which are added may significantly affect the nucleation and growth of the silicate/surfactant assemblies, more-complicated structures were created by varying the size and shape of the silica additives.

Besides the precise structural control over relatively large distances, this method can be extended to synthesize nanowire networks with various chemical compositions such as other metals (e.g. Co), alloys (e.g. PtNi), and semiconductors (CdSe, CdS, and Bi_2Te_3). An example of CdSe nanowire networks is shown in Figure 2, h and i. The images suggest an ordered (Figure 2h) and crystalline (Figure 2i) replicated mesostructure in the semiconductor nanowire networks. The SAED pattern (Figure 2h, inset) indicates a randomly oriented zinc blende crystalline structure. Crystalline CdSe networks composed of ≈11-, 5-, and 3-nm diameter nanowires were synthesized by using cubic templates which offered the corresponding pore diameters. The ability to control the nanowire diameter in turn allows continuously tuned optical absorption owing to quantum confinement. The first excitonic peaks in the absorption spectra of the CdSe nanowire network shift from $\lambda = 640$ to 470 nm upon decreasing the diameters of the nanowire from 11 to 3 nm (Figure 4b). As the nanowires are arranged in a stable network through strong metallic or covalent bonds, as-synthesized networks are stable in organic solvents and remain unaffected after thermal treatments. Crystallized semiconductor nanowire networks with 3D interconnected hierarchical structures and tunable optical properties are great candidates for optical hosts, photovoltaics, and other applications.

Figure 4c shows magnetization hysteresis loops measured at room temperature of a Co 3D nanowire network by using a field applied either parallel or perpendicular to the substrate.

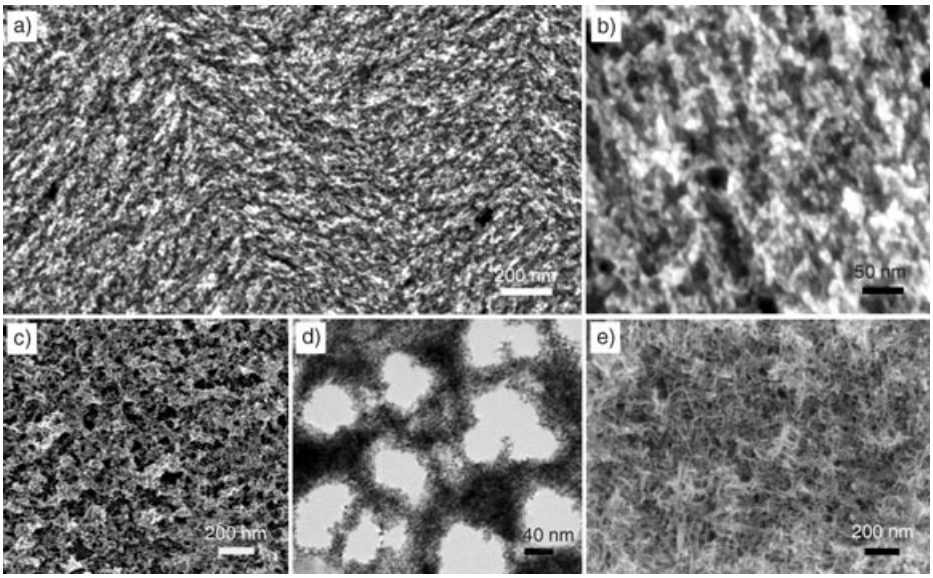

Figure 3. Top-view FESEM and TEM images of Pt nanowire networks of controlled macroscopic morphologies. a) and b) Low- and high-magnification FESEM images of 3D Pt nanowire networks, prepared by using the Brij 58-directed mesoporous silica template, which show homogeneous surface morphology and the ordered mesostructure, respectively. c) and d) FESEM and TEM images of a hierarchically porous Pt nanowire network cotemplated by Brij 58-directed mesoporous silica and dense colloidal silica particles with an average diameter of 20–70 nm. e) FESEM image of a Pt nanowire sponge cotemplated by P123-directed mesoporous silica and dense colloidal silica (70–100 nm). This sponge structure consists of intertwined 3D nanowires that form an interconnected hierarchical pore network.

The presence of the hysteresis loop in both directions indicates that the Co nanowire network is ferromagnetic at room temperature. A higher coercivity (255 Oe) than that of Co thin films (≈10 Oe)[16] is observed. Furthermore, the 3D nanowire network, different from Co thin films or 2D wire arrays with uniaxial anisotropic magnetization,[16,17] gives isotropic magnetism as indicated by its similar coercivity and remanent magnetization behaviors shown in the inset of Figure 4c. In comparison, diluted Co nanoparticles of 2–11-nm diameter and 2D Co nanoparticle superlattices show superparamagnetic behavior at room temperature.[18,19] Such superparamagnetic behavior is due to the randomized particle magnetic polarizations at a temperature higher than the blocking temperature.[18] The unique continuous 3D nanowire network structure may enhance the dipolar interactions between magnetic domains or the intercoupling along nanowire chains, which may result in increased blocking temperatures and room temperature ferromagnetic behavior.[20,21] A 3D Co nanowire network with a smaller diameter of the nanowire (3–4 nm) also shows ferromagnetic behavior at room temperature.[22] Detailed studies are underway to understand fundamentally the magnetic behaviors. Nevertheless, such room temperature ferromagnetic nanowire networks with small nanowire dimensions and enhanced coercivities show potential for high-density information storage applications.

In conclusion, we have developed a rapid and effective approach to fabricate stable macroscopic nanowire networks with controllable composition, tunable hierarchical structure, and unique properties. The dimensions of the nanowire and the network structure are tunable by the precise replication of the self-assembled silica/surfactant liquid-crystalline structure. Hierarchical pore morphology can be obtained by using secondary silica porogens that have desired shapes and sizes. This versatile approach is applicable to a variety of materials such as polymers, metals, and semiconductors. Robust 3D nanowire networks fabricated with this low-cost templated electrodeposition technique are of great interest for photo-

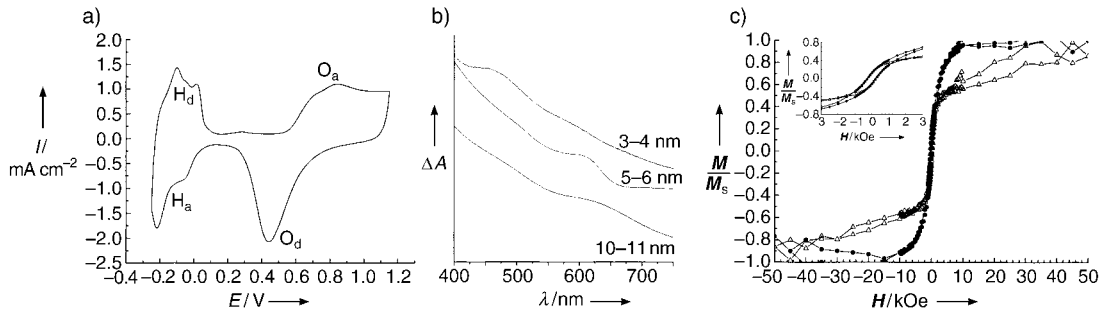

Figure 4. a) Cyclic voltammogram of 3D Pt nanowire networks in sulfuric acid (0.5 M). H_a: hydrogen adsorption, H_d: hydrogen desorption, O_a: adsorption of oxygen, O_d: reduction of oxygen layer. b) UV/Vis spectra of CdSe nanowire networks with various nanowire diameters, which were controlled by the pore diameters of the mesoporous silica templates. Surfactants F127, Brij 58, and CTAB were used to prepare cubic mesoporous templates with pore diameters of 10–11, 5–6, and 3–4 nm, respectively. c) Room temperature magnetization hysteresis loops of 3D Co nanowire networks with a wire diameter of 5–6 nm in an applied field which is either parallel (△) or perpendicular (●) to the substrate. Each curve was normalized to full saturation. The inset shows a hysteresis loop curve indicating near-equal coercivity and remanent magnetization of the Co nanowire network.

voltaic and thermoelectric devices, fuel cells, hydrogen separation membranes, sensors, high-density information storage media, and other device applications.

Experimental Section

Mesoporous silica films were spin- or dip-coated onto conductive glass substrates (ITO (indium tin oxide) or F-doped SnO_2) by using surfactant/silicate sols that were prepared by mixing tetraethoxysilane (TEOS), H_2O, surfactant, HCl, and ethanol in a molar ratio of 1:5:0.02–0.05:0.028:22 at room temperature for 2 h. As-deposited films were calcined in air at 400 °C for 1 h to remove the surfactants and to create mesoporous networks. The nonionic surfactant, Brij 58 ($C_{16}H_{33}(OCH_2CH_2)_{20}OH$), was used as the pore-structure directing agent to synthesize 3D mesoporous templates with pore diameters of 5 nm. Triblock copolymer Pluronic F127 ($EO_{106}PO_{70}EO_{106}$; EO = ethylene oxide, PO = propylene oxide), P123 ($EO_{20}PO_{70}EO_{20}$), and cationic surfactant cetyltrimethylammonium bromide (CTAB) were used to synthesize 3D mesoporous templates with different pore diameters. Commercial solutions (adjusted to pH 1) of dense silica particles with controllable diameters of 20–100 nm were added to the precursor sols to synthesize templates with hierarchical pore structures.

Electrodeposition was conducted in aqueous precursor solutions by using a galvanostatic or potentostatic electroplating circuit in a conventional three-electrode cell. Electrodeposition of Pd was carried out with a periodic galvanostatic pulse current (0.5 mA cm^{-2} for 100 ms and 1 s at 0 mA cm^{-2}) by using an aqueous solution of $PdCl_2$–HCl (0.5 wt.%). Pt deposition was conducted under similar conditions by using a 2-wt.% H_2PtCl_6 precursor solution. Deposition of Co was conducted at −1.2 V vs. SCE by using aqueous solutions containing methanol (20 vol.%), $CoSO_4$ (1.3 M), and H_3BO_3 (0.7 M). Typical CdSe deposition was conducted at 85 °C at −0.65 V vs. SCE by using a deposition solution (pH 2.5) that contained $CdSO_4$ (0.2 M) and SeO_2 (1.0 mM).[23] The electrodeposited films of the metal nanowire networks were annealed at 400 °C in forming gas (N_2 with 10% H_2) for 30 min. The silica templates were removed with HF (1%) or NaOH solution (2 M) at 80 °C, and the networks were rinsed with distilled water. Nanowire networks were characterized by XRD, TEM, SEM, UV/Vis, cyclic voltammetry, and SQUID techniques (see Supporting Information).

Received: May 1, 2004
Revised: July 27, 2004

Keywords: electrochemistry · magnetic properties · mesoporous materials · nanostructures · template synthesis

[1] B. Messer, J. H. Song, P. Yang, *J. Am. Chem. Soc.* **2000**, *122*, 10232.
[2] P. Yang, *Nature* **2003**, *425*, 243.
[3] X. Duan, Y. Huang, Y. Cui, J. Wang, C. M. Lieber, *Nature* **2001**, *409*, 66.
[4] F. X. Redl, K. S. Cho, C. B. Murray, S. O'Brien, *Nature* **2003**, *424*, 968.
[5] S. Sun, C. B. Murray, D. Weller, L. Folks, A. Moser, *Science* **2000**, *287*, 1989.
[6] Y. Huang, X. Duan, Q. Wei, C. M. Lieber, *Science* **2001**, *291*, 630.
[7] O. D. Velev, P. M. Tessier, A. M. Lenhoff, E. W. Kaler, *Nature* **1999**, *401*, 548.
[8] D. Walsh, L. Arcelli, T. Ikoma, J. Tanaka, S. Mann, *Nat. Mater.* **2003**, *2*, 386.
[9] L. Huang, H. Wang, Z. Wang, A. Mitra, K. N. Bozhilov, Y. Yan, *Adv. Mater.* **2002**, *14*, 61.
[10] D. Wang, W. L. Zhou, B. F. McCaughy, J. E. Hampsey, X. Ji, Y.-B. Jiang, H. Xu, J. Tang, R. H. Schmehl, C. O'Connor, C. J. Brinker, Y. Lu, *Adv. Mater.* **2003**, *15*, 130.
[11] Y. Lu, R. Ganguli, C. A. Drewien, M. T. Anderson, C. J. Brinker, W. Gong, Y. Guo, H. Soyez, B. Dunn, M. H. Huang, J. I. Zink, *Nature* **1997**, *389*, 364.
[12] M. Choi, R. Ryoo, *Nat. Mater.* **2003**, *2*, 473.
[13] S. H. Joo, S. J. Choi, I. Oh, J. Kwak, Z. Liu, O. Terasaki, R. Ryoo, *Nature* **2001**, *412*, 169.
[14] G. S. Attard, P. N. Bartlett, N. R. B. Coleman, J. M. Elliott, J. R. Owen, J. H. Wang, *Science* **1997**, *278*, 838.
[15] J. Lee, J. Kim, T. Hyeon, *Chem. Commun.* **2003**, 1138.
[16] T. Thurn-Albrecht, J. Schotter, G. A. Kastle, N. Emley, T. Shibauchi, L. Krusin-Elbaum, K. Guarini, C. T. Black, M. T. Tuominen, T. P. Russell, *Science* **2000**, *290*, 2126.
[17] T. M. Whitney, J. S. Jiang, P. C. Searson, C. L. Chien, *Science* **1993**, *261*, 1316.
[18] S. Sun, C. B. Murray, *J. Appl. Phys.* **1999**, *85*, 4325.
[19] C. T. Black, C. B. Murray, R. L. Sandstrom, S. Sun, *Science* **2000**, *290*, 1131.
[20] J. Garcia-Otero, M. Porto, J. Rivas, A. Bunde, *Phys. Rev. Lett.* **2000**, *84*, 167.
[21] A. F. Gross, M. R. Diehl, K. C. Beverly, E. K. Richman, S. H. Tolbert, *J. Phys. Chem. B* **2003**, *107*, 5475.
[22] H. Luo, D. Wang, V. O. Golub, J. He, Y. Lu, **2004**, unpublished results.
[23] L. Beaunier, H. Cachet, R. Cortes, M. Froment, A. Etcheberry, *Thin Solid Films* **2001**, *387*, 108.

